JOURNAL OF GEOPHYSICAL RESEARCH, VOL. 111, B12S26, doi:10.1029/2006JB004574, 2006

Magnetic petrology of variably retrogressed eclogites and amphibolites: A case study from the Hercynian basement of northern Sardinia (Italy)

Eleonora Strada,[1,2] Franco Maria Talarico,[1] and Fabio Florindo[2]

Received 15 June 2006; revised 15 October 2006; accepted 30 October 2006; published 16 December 2006.

[1] This study constitutes the first attempt to integrate rock magnetism and metamorphic petrology in the Hercynian basement of northern Sardinia. The investigation focused on the magnetic petrology of variably retrogressed eclogites and amphibolites from two suites of basic meta-igneous rocks, which occur along a major tectonic line (Posada-Asinara Line), within a medium-grade (MG) and a high-grade (HG) metamorphic complex. Consistent with petromagnetic results, HG metabasites contain variable amounts of monoclinic pyrrhotite (intergrown with rutile) and titanomagnetite (occurring as inclusions in garnet), abundant ilmenite (associated to secondary hornblende and with sphene ± low-Ti-magnetite rims), and rutile both as inclusions in ilmenite and as discrete grains. In MG metabasites, pyrrhotite is restricted to amphibolites of the Posada Valley area where it occurs as rare inclusions in garnet. All samples are characterized by variable amounts of ilmenite, rutile, and sphene which show the same microstructural features described in HG rocks. Microstructural evidence and geothermobarometric data indicate that (1) pyrrhotite and titanomagnetite likely formed prior to and remained stable during the eclogite facies metamorphic peak and (2) the growth of ilmenite and sphene can be attributed to the amphibolite facies retrogression, mainly due to model reactions such as garnet + omphacite + rutile + H_2O → hornblende + plagioclase + ilmenite and amphibole + ilmenite + O_2 → sphene + magnetite + quartz + H_2O. The results from our combined petrological and petromagnetic study corroborate the hypothesis that significant volumes of mafic/ultramafic rocks, similar to some of the investigated outcrops, may account for the magnetic anomalies flanking the northeastern part of the Posada-Asinara Line.

Citation: Strada, E., F. M. Talarico, and F. Florindo (2006), Magnetic petrology of variably retrogressed eclogites and amphibolites: A case study from the Hercynian basement of northern Sardinia (Italy), *J. Geophys. Res.*, *111*, B12S26, doi:10.1029/2006JB004574.

1. Introduction

[2] The silicate parageneses of variably retrogressed eclogites are extensively used by metamorphic petrologists to reconstruct the tectonometamorphic evolution of ophiolites-bearing units and high-pressure continental tectonic slices in orogenic belts from initial burial to exhumation. On the other hand, the opaque mineralogy of these rocks is generally not studied in detail although the characterization of Fe-Ti oxides and sulphides in metabasites has a great potential [*Clark*, 1997; *Dunlop and Özdemir*, 1997; *Frost*, 1991b] to better understand the processes controlling the formation and stability of magnetic minerals (mainly magnetite and pyrrhotite) in subduction zones and collisional orogens and to improve geological interpretation of magnetic survey data.

[3] The Hercynian basement of northern Sardinia provides a case study to define the relationships between metamorphic evolution and magnetic properties of eclogite and amphibolite facies metabasites in a number of structurally and petrologically well-studied outcrops within a representative crustal section of the southern European Variscan belt.

[4] To characterize the magnetic properties of these rocks, we conducted a series of minero-petrographical analyses and mineral magnetic measurements on a suite of samples representative of all the main mafic/ultramafic lenses of the region. In this study, we report on new data and interpretations which are essential (1) to characterize and to verify primary and secondary oxide contributions to the overall magnetization, (2) to link the stability/instability of magnetic assemblages to specific metamorphic stages, and (3) to provide a preliminary regional-scale perspective on the level of magnetization in all the main metamorphic mafic rock units of the Hercynian orogenic belt in northern Sardinia.

2. Geological Setting

[5] The Sardinia-Corsica lithospheric block (Figure 1) represents a microplate which was separated from the European margin as a result of the opening of the Liguro-

[1]Dipartimento di Scienze della Terra, Università di Siena, Siena, Italy.
[2]Istituto Nazionale di Geofisica e Vulcanologia, Rome, Italy.

0148-0227/06/2006JB004574$09.00

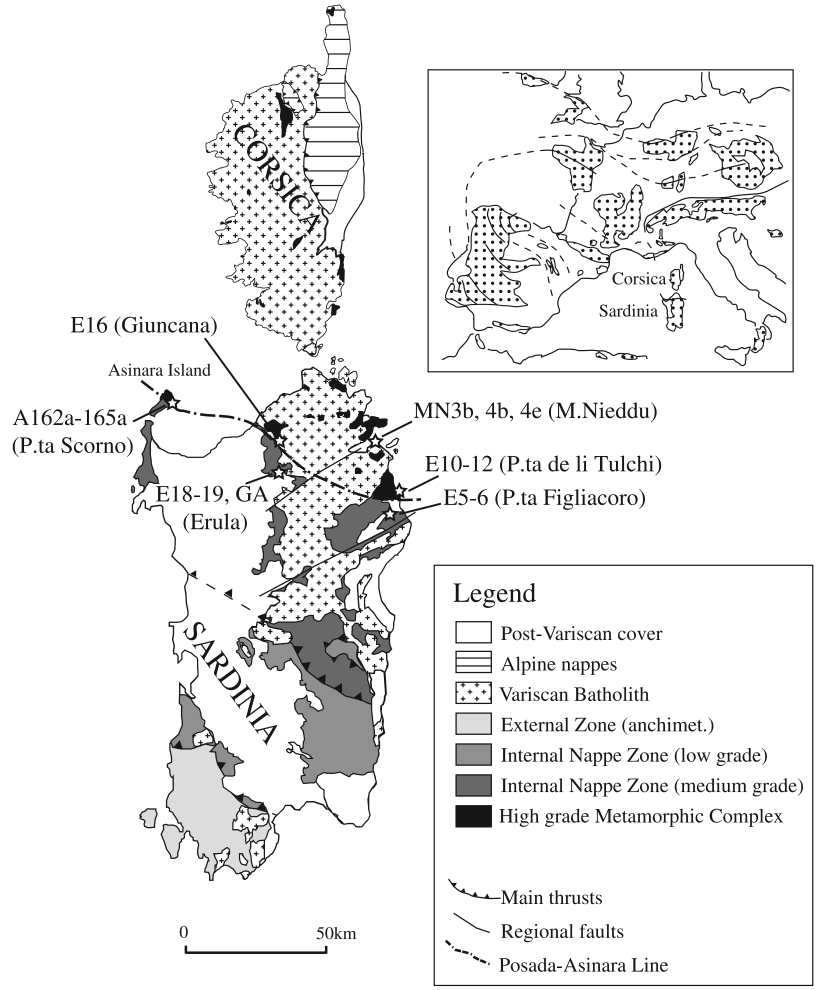

Figure 1. Simplified geological map of Sardinia and Corsica islands (modified after *Giacomini et al.* [2005] and *Carosi and Palmeri* [2002]) and their actual position (upper right) with respect to the European Variscides (dotted, modified after *Stampfli et al.* [2002]).

Provençal Basin in late Oligocene–early Miocene times [*Arthaud and Matte*, 1977; *Speranza et al.*, 2002]. The Sardinia crystalline basement (Figure 1) constitutes a section of the southern sector of the European Variscan belt [*Menot and Orsini*, 1990] and it comprises three main tectonometamorphic complexes [*Carmignani et al.*, 1994, and references therein] including (1) a foreland "thrusts and folds" belt (SW Sardinia), mainly constituted by fold and thrust anchimetamorphic sedimentary sequences of Cambro-Carboniferous age; (2) a SW verging nappe zone (central Sardinia), of low- to medium-grade metamorphosed sedimentary (Paleozoic) and volcano-sedimentary (early Ordovician to Caradocian) sequences; (3) an inner zone ("axial zone") (northeastern Sardinia and southern Corsica) characterized by medium- to high-grade metamorphic rocks which experienced a polyphase tectonometamorphic evolution and Barrovian type metamorphism [*Ferrara et al.*, 1978; *Franceschelli et al.*, 1982, *Elter et al.*, 1986; *Carmignani et al.*, 1992; *Ricci*, 1992] followed by the emplacement of a late to post tectonic high-K calc-alkaline intrusions (310 to 280 Ma) including both strongly peraluminous granitoids [*Di Vincenzo et al.*, 1994, and references therein] and 280–290 Ma posttectonic leucogranites [*Di Vincenzo et al.*, 1994; *Carmignani and Rossi*, 1999].

[6] According to *Carmignani et al.* [1994] the axial zone is subdivided into two different complexes separated by a prominent and several kilometers wide mylonitic belt (Posada-Asinara Line), characterized by a polyphased structural evolution [*Elter et al.*, 1986] and by the occurrence of several mafic lenses including mid-ocean ridge basalt-type (MORB) amphibolites and eclogites [*Cortesogno et al.*, 2004]. These include (1) a medium-grade metamorphic complex (medium-grade Internal Nappe Zone, Figure 1) composed of dominant metapelites, metasandstones and quartzites, metamorphosed under intermediate pressure greenschist to amphibolite facies conditions; and (2) a high-grade metamorphic complex mainly consisting of amphibolite facies migmatites and orthogneisses ranging in age from 440 to 490 Ma [*Ferrara et al.*, 1978; *Cruciani et al.*, 2003; *Helbing*, 2003], and scattered mafic bodies retaining granulite and/or eclogite facies relic assemblages [*Miller et al.*, 1976; *Ghezzo et al.*, 1979; *Franceschelli et al.*, 1998]. The Posada-Asinara Line has been differently interpreted either as a Hercynian suture zone, separating the pre-Cambrian Armorican continental margin from

Gondwana [*Cappelli et al.*, 1992; *Carmignani et al.*, 1992], or as a wide Variscan transpressional shear belt [*Carosi and Palmeri*, 2002]. Additional geological and geochronological evidence corroborating the absence of a "suture zone" in northeastern Sardinia has recently been provided by *Helbing* [2003].

[7] Investigated samples are representative of two suites of metabasites, both consisting of eclogites, retrogressed eclogites and amphibolites: (1) several meters to 150-m-thick lenses hosted in migmatitic gneisses of the High-grade Metamorphic Complex (as defined by *Carmignani et al.* [1994]), and (2) smaller (up to 50 m thick) lenses contained within kyanite-bearing biotite-muscovite schists of the medium-grade Internal Nappe Zone [*Carmignani et al.*, 1994] within, or a few kilometers south of, the Posada-Asinara Line (Figure 1).

3. Analytical Methods

3.1. Field Measurements

[8] Bulk magnetic susceptibility measurements with a portable kappameter have been recorded for each outcrop. We used an AGICO (ex Geofyzika Brno) KT-5 Kappameter of pocket size (diameter 66 mm) with a maximum sensitivity of 1×10^{-5} SI units. This hand-held instrument is calibrated for the pick-up coil in contact with an absolutely smooth plane confining a half-space filled with magnetically homogeneous and isotropic medium. For practical purpose, a sufficient accuracy can be obtained with samples with thickness >50 mm and diameter >100 mm and smooth surfaces with unevenness <1 mm. Out of these ranges, measured values should be multiplied by the respective correction factor following the manufacture specifications. According to experimental results [*Lecoanet et al.*, 1999], the instrument is characterized by a quite symmetrical data acquisition feature and by a shallow effective penetration depth: 90% of the magnetic signal is integrated in the first 2.3 cm and 95% in the first 3 cm. Calibration tests on unweathered rocks showed that measured susceptibility data are very close to the true values [*Lecoanet et al.*, 1999].

3.2. Petromagnetic Laboratory Investigations

[9] The carriers of magnetization and their distribution within selected samples are described using a set of rock magnetic analyses (low-field magnetic susceptibility, natural and artificial remanences, thermomagnetic analyses, hysteresis loops, coercivity of remanence). All these analyses were performed at the paleomagnetism laboratory of the Istituto Nazionale di Geofisica e Vulcanologia (INGV) in Rome. Low-field magnetic susceptibility measurements were made in laboratory using a KLY 2 (AGICO) Kappabridge (noise level 2×10^{-10} m^3 kg^{-1}). Because of the irregular shape of the samples we normalized these measurements to a given mass. Natural and artificial magnetizations were measured using a pass-through cryogenic magnetometer by 2G Enterprises (model 750R) with internal diameter of 4.2 cm, equipped with three DC SQUID sensors (noise level 3×10^{-9} A m^2 kg^{-1}). This instrument has in-line static demagnetization capability, with possibility to impart a direct field for the acquisition of an anhysteretic remanent magnetization (ARM). The ARM was imparted using a direct current (DC) bias field of 0.05 mT superimposed on a 100 mT peak AF, which was gradually reduced to zero. An in-line pulse magnetizer allows the application of impulsive magnetic field up to 0.9 T to study the isothermal remanent magnetization (IRM). For samples with very high intensities of magnetization, we used a JR-5A spinner magnetometer (noise level 5×10^{-11} A m^2).

[10] Hysteresis properties were investigated using a Molspin vibrating sample magnetometer (VSM) with up to 1 T field application. Backfields from saturation were used to determine the coercivity of remanence (B_{cr}).

[11] For discriminating ferromagnetic mineralogy, the temperature dependence of the magnetic susceptibility, up to maximum temperature of 700°C, was measured with a furnace-equipped KLY 3 (AGICO) Kappabridge (noise level 2×10^{-8} SI). For selected samples we studied thermomagnetic properties in an argon atmosphere flow in order to minimize mineral reactions with atmospheric oxygen that may occur during the heating process.

3.3. Mineral Chemistry and Backscattered Electron Images

[12] Mineral analyses were carried out using a JEOL JX 8600 electron microprobe fitted with four wavelength-dispersive spectrometers, at the Centro Studi per la Minerogenesi e la Geochimica Applicata (CNR-Florence), operating with an accelerating voltage of 15 kV and 10 nA sample current using natural minerals as standards. Backscattered electron images and scanning electron microscope–energy dispersive spectrometer (SEM-EDS) qualitative determinations of opaque minerals were performed using a Philips 515 scanning electron microscope with the EDAX 9100/70 X-ray energy dispersive system, running at 15 kV and with an emission current of 20 nA, at the Dipartimento di Scienza della Terra dell'Universitá di Siena.

4. Field and Petrographical Features of the Samples

[13] In the following descriptions, we use the term "eclogite" for the samples characterized by the best preserved eclogitic relics, which are nevertheless only represented by rare millimeter-scale relics of omphacite occurring as inclusions in garnet porphyroblasts within strongly reequilibrated domains. We classified as "retrogressed eclogites" the varieties of eclogites which have been amphibolitized but still retain some textural (i.e., symplectites) evidence of a former eclogitic stage. Finally, we restrict the use of "amphibolite" to indicate all the rocks that do not contain either textural (i.e., symplectites) or mineralogical (i.e., paragenetic relics) evidence of a former eclogitic stage. Representative analyses of Fe-Ti oxides in the investigated samples are reported in Table 1. Mineral abbreviations are according to *Kretz* [1983] and amphibole nomenclature is after *Leake et al.* [1997].

4.1. High-Grade Metamorphic Complex

[14] Samples for petromagnetic investigations were collected in 3 areas including Punta de Li Tulchi, Golfo Aranci (Montiggiu Nieddu), and Punta Scorno at the northern tip of the Asinara Island (Figure 1).

[15] Consistent with petromagnetic results and their variable magnetic susceptibilities (as detailed below), HG

Table 1. Selected Electron Microprobe Analyses and Structural Formulae of Oxide Minerals[a]

	E10							E12			MN4				E16			E18			E6	
	Mt S5-opm 3-c	Ti-Mt S5-opm 10-c	Mt S5-opm 11-c	Ilm S5-opm 14-c	Ilm S2-opm 3-c	Ilm S5-opm 15-c	Ilm S2-opm 10-c	Ilm S3-opm 2-c	Ilm S3-opm 3-c	Ilm S2-opm 5-c	Mt S1-opm3	Mt s2-opm2	Ilm S1-opm5	Ilm s2-opm1	Ilm S4-opm1	Ilm S3-opm1	Ilm S2-opm1	Ilm S1-opm2	Ilm S1-opm3	Ilm S2-opm2	Ilm S2-opm3	Ilm S1-opm3
SiO_2	0.00	0.00	0.00	0.00	0.68	0.00	0.78	0.00	0.00	0.00	0.66	2.81	0.56	0.39	0.18	0.41	0.52	0.38	0.43	0.56	0.19	0.67
TiO_2	0.67	25.12	6.12	52.39	48.22	52.59	46.50	52.40	51.94	53.10	0.42	0.16	48.26	51.59	48.92	51.60	47.16	49.95	49.75	49.01	47.97	48.38
Al_2O_3	0.00	0.00	0.00	0.00	0.49	0.00	0.76	0.00	0.00	0.00	0.40	0.72	0.44	0.39	0.20	0.18	0.36	0.10	0.32	0.51	0.23	0.28
Cr_2O_3	0.73	0.22	0.21	0.00	0.00	0.00	0.00	0.00	0.12	0.00	0.42	0.00	0.00	0.00	0.00	0.11	0.13	0.00	0.00	0.00	0.12	0.00
Fe_2O_3	67.40	20.77	57.17	2.01	8.10	0.47	12.88	1.11	2.22	0.24	66.56	63.39	7.75	2.34	8.37	1.76	11.50	4.93	5.22	7.64	10.99	6.59
FeO	30.67	53.67	35.98	44.35	40.73	45.37	36.84	44.54	42.90	44.77	29.75	31.38	41.04	43.96	40.44	44.06	36.62	43.16	42.30	39.78	37.64	41.44
MnO	0.16	0.25	0.08	0.07	1.10	0.62	0.70	1.42	2.37	2.05	0.51	0.17	1.10	0.48	0.59	1.23	2.30	1.24	1.34	1.05	1.75	2.32
MgO	0.33	0.11	0.25	1.43	0.28	0.49	0.74	0.52	0.50	0.25	0.52	0.52	0.32	0.29	0.54	0.00	0.52	0.11	0.31	0.70	0.24	0.00
CaO	0.00	0.00	0.00	0.00	0.19	0.00	0.00	0.00	0.00	0.00	0.39	0.25	0.31	0.18	0.34	0.38	0.18	0.13	0.19	0.20	0.24	0.23
Na_2O	0.00	0.00	0.00	0.00	0.22	0.00	0.75	0.00	0.00	0.00	0.00	0.52	0.14	0.30	0.27	0.14	0.51	0.13	0.10	0.49	0.66	0.00
K_2O	0.00	0.00	0.00	0.00	0.16	0.00	0.07	0.00	0.00	0.00	0.28	0.07	0.10	0.09	0.18	0.15	0.18	0.00	0.11	0.04	0.05	0.07
ZnO	0.25	0.29	0.18	0.09	0.04	0.23	0.11	0.12	0.29	0.25	0.00	0.00	0.00	0.00	0.00	0.00	0.00	0.00	0.00	0.00	0.00	0.00
Total	100.22	100.43	99.98	100.34	100.21	99.78	100.13	100.11	100.34	100.67	99.92	99.98	100.01	100.01	100.01	100.01	99.98	100.12	100.07	99.97	100.08	99.98
Si	0.000	0.000	0.000	0.000	0.017	0.000	0.019	0.000	0.000	0.000	0.025	0.105	0.014	0.010	0.004	0.010	0.013	0.010	0.011	0.014	0.005	0.017
Al	0.000	0.000	0.000	0.000	0.014	0.000	0.022	0.000	0.000	0.000	0.018	0.032	0.013	0.011	0.006	0.005	0.010	0.003	0.009	0.015	0.007	0.008
Ti	0.019	0.705	0.176	0.981	0.907	0.996	0.868	0.990	0.978	0.998	0.012	0.004	0.911	0.971	0.923	0.975	0.887	0.946	0.939	0.919	0.904	0.918
Cr	0.022	0.006	0.006	0.000	0.000	0.000	0.000	0.000	0.002	0.000	0.013	0.000	0.000	0.000	0.000	0.002	0.003	0.000	0.000	0.000	0.002	0.000
Fe3+	1.939	0.583	1.642	0.038	0.152	0.009	0.241	0.021	0.042	0.005	1.908	1.789	0.146	0.044	0.158	0.033	0.217	0.093	0.099	0.143	0.207	0.125
Fe2+	0.981	1.675	1.149	0.924	0.852	0.955	0.765	0.935	0.898	0.936	0.948	0.984	0.862	0.920	0.848	0.926	0.766	0.908	0.888	0.830	0.789	0.874
Mn	0.005	0.008	0.002	0.001	0.023	0.013	0.015	0.030	0.050	0.043	0.017	0.005	0.023	0.010	0.012	0.026	0.049	0.026	0.029	0.022	0.037	0.050
Mg	0.019	0.006	0.014	0.053	0.010	0.018	0.027	0.020	0.019	0.009	0.030	0.029	0.012	0.011	0.020	0.000	0.020	0.004	0.012	0.026	0.009	0.000
Ca	0.000	0.000	0.000	0.000	0.005	0.000	0.000	0.000	0.000	0.000	0.016	0.010	0.008	0.005	0.009	0.010	0.005	0.003	0.005	0.005	0.006	0.006
Na	0.000	0.000	0.000	0.000	0.011	0.000	0.036	0.000	0.000	0.000	0.000	0.037	0.007	0.015	0.013	0.007	0.025	0.006	0.005	0.024	0.032	0.000
K	0.000	0.000	0.000	0.000	0.005	0.000	0.002	0.000	0.000	0.000	0.014	0.003	0.003	0.003	0.006	0.005	0.006	0.000	0.004	0.001	0.002	0.002
Zn	0.014	0.016	0.010	0.003	0.001	0.009	0.004	0.004	0.011	0.009	0.000	0.000	0.000	0.000	0.000	0.000	0.000	0.000	0.000	0.000	0.000	0.000
Total	3.000	3.000	3.000	2.000	2.000	2.000	2.000	2.000	2.000	2.000	3.000	3.000	2.000	2.000	2.000	2.000	2.000	2.000	2.000	2.000	2.000	2.000

[a]Ilm, ilmenite; Mt, magnetite; Ti-Mt, titanomagnetite in northern Sardinia metabasites.

(high-grade) eclogites contain: variable contents of monoclinic pyrrhotite (intergrown with rutile) occurring as mm grains within the symplectite-rich domains; rare titanomagnetite, occurring as inclusions in garnet; rutile both as inclusions in ilmenite and as discrete grains. All investigated metabasites (including eclogites, retrogressed eclogites and amphibolites, a part from the Punta Scorno ones) are characterized by abundant ilmenite associated to secondary hornblende and plagioclase, and at places (Montiggiu Nieddu) rimmed by sphene ± low-Ti magnetite.

[16] In the Punta de Li Tulchi area, eclogite (E10) and retrogressed eclogite (E12) were sampled from a ~20-m-thick lens hosted in migmatitic orthogneisses. The main foliation strikes 60°/350° (angle of dip/dip direction) and it is defined by the alternation of garnet-rich layers and hornblende-rich layers. In sample E10, relics of omphacite (jd_{28} acm_{27}) occur within large, several millimeters wide porphyroblasts of garnet ($prp_{22\text{-}22}$ $alm_{53\text{-}57}$ $sps_{2\text{-}1}$ $grs_{23\text{-}21}$) which are surrounded by a thin corona of plagioclase ($an_{35\text{-}40}$ $ab_{64\text{-}60}$ $or_{1\text{-}0}$) ± Mg-hornblende and opaque minerals (Figure 2a) and set in a slightly foliated matrix consisting of symplectites after pristine omphacite (albite + diopside with very low jadeite (0.4–0.6 mol %) and acmite (0–0.06 mol %) contents), Mg-hornblende, rutile and pyrrhotite (Figures 2a and 2b). Rare Ti-magnetite occurs as inclusion in garnet and in the symplectites. Opaque minerals in the coronas are nearly pure magnetite or ilmenite, with variable composition for Mn (MnO = 0.07–1.10 wt %) and Fe_2O_3 (0.47–12.88%) (Table 1 and Figure 3). The highest MnO and Fe_2O_3 contents are shown by grains enclosed in garnet and close to magnetite, respectively.

[17] Sample E12 is characterized by poorly preserved anhedral garnet crystals (weakly zoned with prp_{30} alm_{51} sps_3 grs_{16} cores, and prp_{24} alm_{57} sps_2 grs_{17} rims) rimmed by plagioclase ($an_{28\text{-}2}$ $ab_{71\text{-}93}$ $or_{1\text{-}5}$) (Figure 2c) and by a higher modal content in Mg-hornblende, at places occurring as polycrystalline aggregates with inclusions of ilmenite (MnO = 1.42–2.37 wt % and Fe_2O_3 = 0.24–2.22 wt %, Figure 3) sometimes intergrown with rutile (Figure 2d) or rimmed by sphene.

[18] In the Montiggiu Nieddu area, samples MN3b, MN4b, and MN4e were collected from a ~150-m-thick layered lens, trending N-S/NNW-SSE and often subvertical or steeply east dipping, and hosted in migmatitic paragneisses, at places with nebulitic-agmatitic textures, with rare small calc-silicate nodules and felsic orthogneiss bodies (mainly two micas and K-feldspar gneisses with augen texture).

[19] The Montiggiu Nieddu lens consists of plagioclase-rich amphibolites interlayered with amphibolitized ultramafic rocks (including horneblendites and olivine ± pyroxene bearing varieties) which, according to *Ghezzo et al.* [1979] and *Franceschelli et al.* [2002], can be interpreted as cumulate layers, indicating an original intrusive nature of the whole mafic sequence. Amphibolite MN4b is representative of the plagioclase-rich varieties and it shows a nematoblastic texture defined by the preferred dimensional orientation of tschermakite, with pyrite and ilmenite inclusions, and rare subhedral crystals of garnet (prp_{21} alm_{54} sps_6 grs_{19}), occurring as inclusion in plagioclase (Figure 2e). Plagioclase shows variable compositions ($an_{77\text{-}51}$ $ab_{23\text{-}48}$ $or_{0\text{-}1}$) depending on its microstructural position: crystals close to garnet are more anorthite rich than the ones close or in contact with partially sphene-substituted ilmenite. In this sample ilmenite grains show internal bands and patches of sphene which also forms thin coronas with sparse grains of low-Ti magnetite (TiO_2 = 0.16–0.42 wt %) (Figures 2f and 2g). Ilmenite compositions are characterized by low Mn contents (MnO = 0.48–1.10 wt %) and variable Fe_2O_3 contents (2.34–7.75 wt %) (Table 1 and Figure 3).

[20] The geological setting of Punta Scorno metabasites closely matches the features of the Montiggiu Nieddu area. Metabasites form an ~100-m-thick and NW-SE trending layered lens hosted in dominant sillimanite-cordierite-bearing migmatitic paragneiss and mylonitic orthogneisses. According to *Carmignani et al.* [1994] and *Castorina et al.* [1996] Punta Scorno amphibolites are geochemically comparable to the Montiggiu Nieddu metabasites. Similar to the Montiggiu Nieddu sample, the samples selected for this study (A165a, A162a) show a marked foliation defined by pale green amphibole (Mg-hornblende/actinolite) and plagioclase ($an_{91\text{-}89}$ $ab_{9\text{-}11}$) (Figure 2h), but they differ for the occurrence of rare biotite lepidoblasts (Figure 2h). Opaque minerals were not detected at either optical or electron microscope observations, but the occurrence of monoclinic pyrrhotite and of magnetite is suggested by petromagnetic experiments.

4.2. Medium-Grade Internal Nappe Zone

[21] In this metamorphic complex we have investigated the eclogite lens of Giuncana (E16), the amphibolites of Erula (E18, E19, GA) and the garnet-bearing amphibolites from Punta Figliacoro in the Posada Valley (E5–E6) (see location in Figure 1).

[22] In these metabasites rutile is restricted to eclogites, whereas pyrrhotite was found only as rare inclusions in garnet or grains close to the margin of garnet porphyroblasts in Punta Figliacoro amphibolites. Ilmenite and sphene were observed in all samples, with microstructural features similar to those described in HG rocks.

[23] Giuncana eclogites constitute a 15-m-thick lens striking 70°/190° within biotite-kyanite-garnet micaschists. Compared to the HG eclogites, Giuncana eclogites are slightly better preserved with relict omphacite (jd_{33} acm_9) and thinner coronas of plagioclase (an_2 ab_{97} or_1) around garnet porphyroblasts. Rutile, intergrown with ilmenite, commonly occurs as inclusions in Mg-hornblende and in the symplectite domains consisting of diopside ($jd_{1\text{-}2.5}$ $acm_{0\text{-}1,3}$) and albite (Figure 4a). Ilmenite grains shows variable shapes (from anhedral to mainly subhedral) and grain size (the smallest individuals forming grape-like aggregates), associated to matrix amphibole and as inclusions, intergrown with amphibole and plagioclase (an_{10} ab_{89} or_1), in the cores of partially preserved garnets. Both rutile and ilmenite are rimmed by sphene (Figure 4b). Similar to HG eclogites, ilmenite shows variable composition for Mn (MnO = 0.59–2.30 wt %) and Fe_2O_3 (1.76–11.50%) (Table 1 and Figure 3), with the highest MnO and Fe_2O_3 contents restricted to grains enclosed in garnet.

[24] Amphibolites E18, E19, and GA (Erula) were sampled from the core of a small, ~5-m-thick lens, striking 70°/260° and hosted in muscovite-rich paragneisses. Sample E18 shows a weak foliation and millimeter-sized aggregates of plagioclase (an_{48} ab_{51} or_1) and Mg-hornblende, most likely the product of pseudomorphic transformation of former

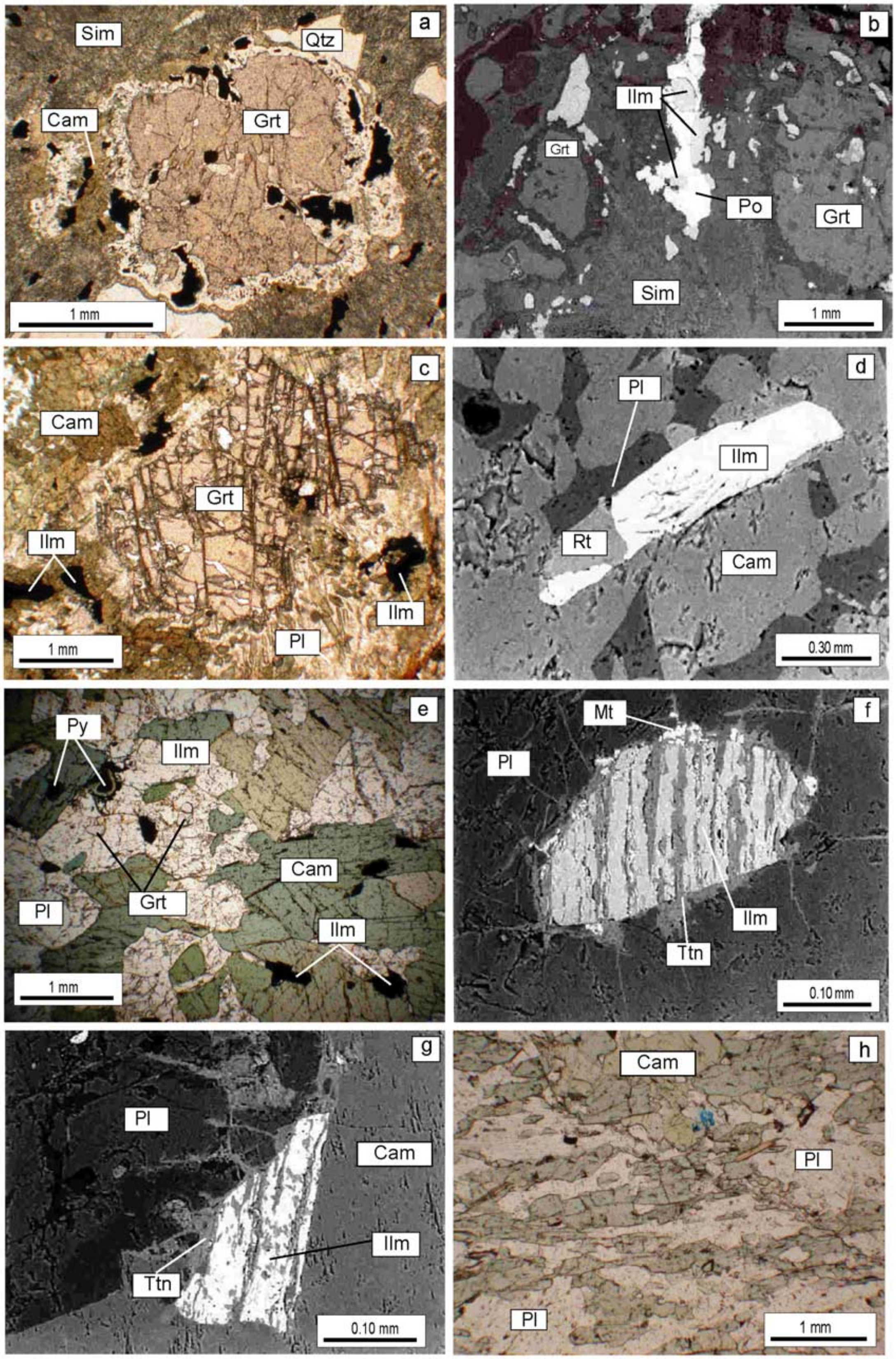
a
Sim
Qtz
Cam
Grt
1 mm
b
Ilm
Grt
Po
Grt
Sim
1 mm
c
Cam
Grt
Ilm
Ilm
Pl
1 mm
d
Pl
Ilm
Rt
Cam
0.30 mm
e
Py
Ilm
Cam
Pl
Grt
Ilm
1 mm
f
Mt
Pl
Ilm
Ttn
0.10 mm
g
Pl
Cam
Ilm
Ttn
0.10 mm
h
Cam
Pl
Pl
1 mm

Figure 2

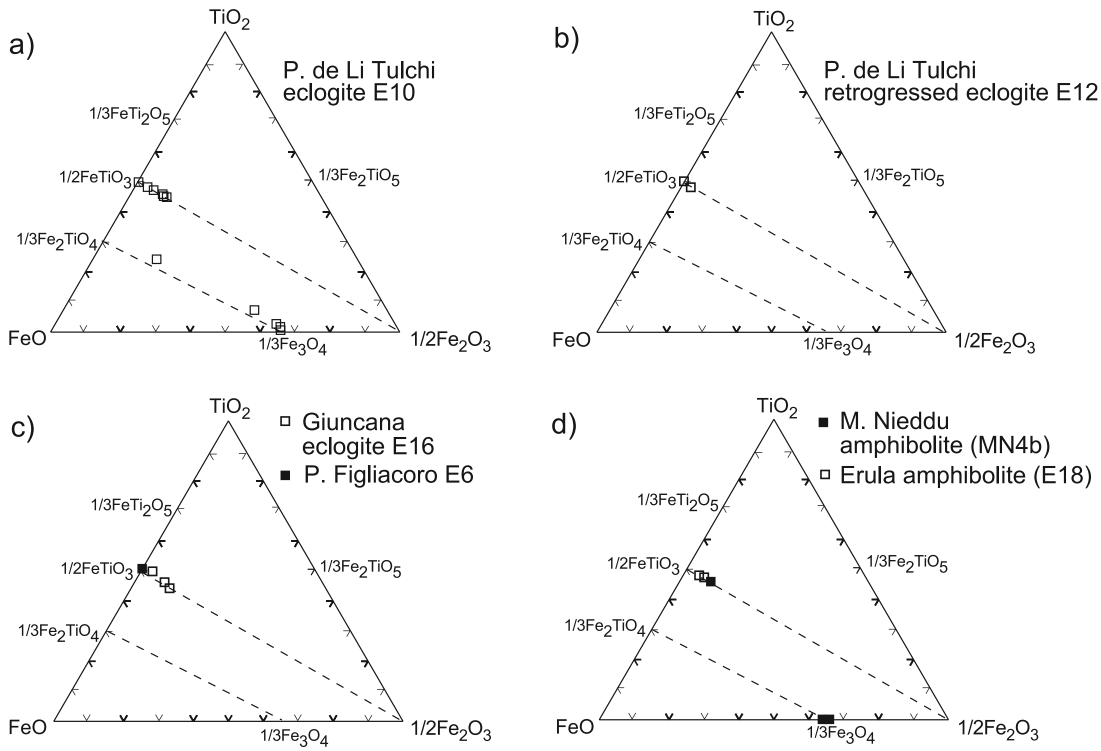

Figure 3. Composition of Fe-Ti oxides (mol %) in northern Sardinia samples plotted on ternary system FeO-Fe_2O_3-TiO_2.

garnet porphyroblasts (Figure 4c). Ilmenite, with varying Mn and Fe^{3+} contents (MnO = 1.05–1.34 wt %; Fe_2O_3 = 4.93–7.64 wt %) (Table 1 and Figure 3), is the ubiquitous and unique opaque mineral in this rock (Figure 4d).

[25] Punta Figliacoro garnet-bearing amphibolites (E5–E6) are from a 7-m-thick lens, striking 78°/166° and hosted in muscovite-rich gneisses. The lens is characterized by a mineralogical layering defined by variation in modal contents of garnet and plagioclase. These rocks show anhedral garnet porphyroblasts with discontinuous coronas of plagioclase ($an_{35\text{-}37}$ $ab_{64\text{-}62}$ $or_{1\text{-}1}$) and set in a nematoblastic matrix of Fe-tschermakite to Fe/Mg-hornblende and plagioclase ($an_{25\text{-}26}$ $ab_{74\text{-}73}$ $or_{1\text{-}1}$) (Figure 4e). Opaque minerals include pyrrhotite, as discrete grains enclosed in garnet or in hornblende close to garnet margins (Figure 4f), and ilmenite, characterized by varying Mn and Fe^{3+} contents (MnO = 1.75–2.32 wt %; Fe_2O_3 = 6.59–10.99 wt %) (Table 1 and Figure 3). Ilmenite is often intergrown with hornblende and plagioclase (Figure 4g) and, at places, rimmed by sphene (Figure 4h).

5. P-T Conditions of Amphibolite Facies Metamorphism

[26] Magnetite compositions very close to the Fe_3O_4 end-member did not allow the use of Fe-Ti oxides for P-T determinations, and the *Buddington and Lindsley* [1964] geothermometer based on the Fe_2TiO_4 content in magnetite coexisting with ilmenite, could not be applied.

[27] Nevertheless, microstructural evidence suggest that the crystallization of ilmenite, the most ubiquitous and abundant among the opaque minerals, may have been coeval

Figure 2. Photomicrographs of investigated samples of metabasites from the High-Grade Metamorphic Complex of NE Sardinia. (a) Garnet (Grt) porphyroblast surrounded by a plagioclase-rich corona with Ca-amphibole (Cam) and ilmenite within a symplectite-rich matrix (Sim) (eclogite E10, plane-polarized light (PPL)); (b) pyrrhotite (Po) rimmed by discrete grains of ilmenite (Ilm) within a Ca-amphibole (Cam)-plagioclase (Pl)-symplectite (Sim) matrix (eclogite E10, backscattered electron image (BSE)); (c) poorly preserved anhedral garnet (Grt) crystal rimmed by plagioclase and ilmenite (Ilm) within a polycrystalline aggregate of Ca-amphibole (Cam) (retrogressed eclogite E12, PPL); (d) ilmenite (Ilm) intergrown with rutile (Rt) (retrogressed eclogite E12, BSE); (e) Ca-amphibole (Cam) nematoblasts with pyrite (Py) and ilmenite (Ilm) inclusions and rare garnet (Grt) subhedral crystals as inclusions in plagioclase (Pl) (amphibolite MN4b, PPL); (f) ilmenite (Ilm) crystal in plagioclase (Pl) shows internal patches and a thin corona of sphene (Ttn) with sparse grains of low-Ti magnetite (Mt) (amphibolite MN4b, BSE); (g) ilmenite (Ilm) crystal, partially replaced by sphene (Ttn) within Ca-amphibole (Cam) close to plagioclase (Pl) (amphibolite MN4b, BSE); (h) Ca-amphibole (Cam) nematoblasts and plagioclase (Pl) define a well-developed schistosity in amphibolite A165a (PPL).

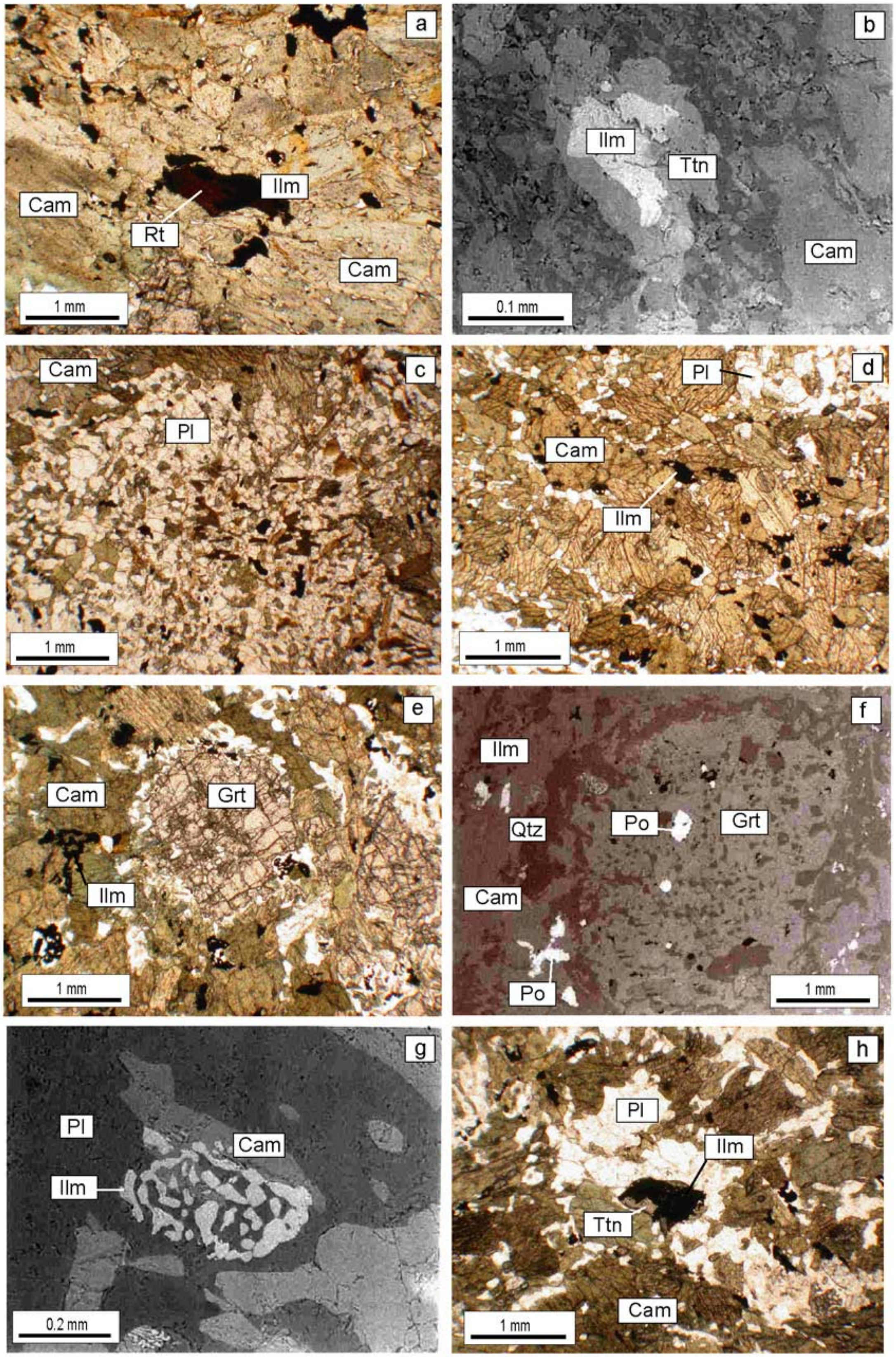
a
Ilm
Cam
Rt
Cam
1 mm
b
Ilm
Ttn
Cam
0.1 mm
Cam
c
Pl
1 mm
Pl
d
Cam
Ilm
1 mm
e
Cam
Grt
Ilm
1 mm
f
Ilm
Qtz
Po
Grt
Cam
Po
1 mm
g
Pl
Cam
Ilm
0.2 mm
h
Pl
Ilm
Ttn
Cam
1 mm

Figure 4

Table 2. P-T Estimates Based on the Empirical Ca-Amphibole Geothermobarometer[a]

Sample	min T (±37°C), min P (±0.12 GPa)	max T (±37°C), max P (±0.12 GPa)
E6	565, 0.55 (Si: 6,755; Al: 2,017; Fe^{3+}: 0,041)	674, 1.02 (Si: 5,574; Al: 3,550; Fe^{3+}: 2,564)
E18	497, 0.40 (Si: 7,087; Al: 1,127; Fe^{3+}: 1,183)	549, 0.5 (Si: 6,844; Al: 1,587; Fe^{3+}: 0,697)
E16	515, 0.45 (Si: 7,321; Al: 0,924; Fe^{3+}: 1,438)	573, 0.53 (Si: 7,011; Al: 1,568; Fe^{3+}: 0,261)
E10	532, 0.45 (Si: 6,983; Al: 1,301; Fe^{3+}: 0,912)	677, 0.80 (Si: 6,052; Al: 2,819; Fe^{3+}: 0,480)
E12	456, 0.28 (Si: 7,452; Al: 0,835; Fe^{3+}: 0,198)	684, 0.84 (Si: 5,949; Al: 2,998; Fe^{3+}: 0,308)
MN4b	611, 0.72 (Si: 6,373; Al: 2,450; Fe^{3+}: 0,874)	642, 0.73 (Si: 6,198; Al: 2,496; Fe^{3+}: 0,843)
A165a	451, 0.27 (Si: 7,515; Al: 0,878; Fe^{3+}: 0,000)	467, 0.29 (Si: 7,420; Al: 1,007; Fe^{3+}: 0,000)

[a]See *Zenk and Schulz* [2004]. Ca-amphibole compositional parameters (Si, Al, Fe^{3+}) used in the calculations are given between brackets as number of cations normalized to 23 oxygens and sum (T1 + T2 + M1 + M2 + M3) = 13 as detailed by *Triboulet* [1992], with Fe^{3+} estimated as maximum according to *Papike et al.* [1974].

with calcic amphibole and plagioclase, which are often intimately intergrown with ilmenite suggesting possible thermodynamic equilibrium conditions for these minerals.

[28] The composition of amphibole coexisting with plagioclase is a good tool to estimate P-T conditions attending the formation of these parageneses. Actually, Si, Al, and Na distribution in structural sites of amphibole depends on physical conditions during crystallization. While Si^{4+} decreases, Ti, ^{VI}Al, and Na_A increase with temperature, and ^{IV}Al and Na_{M4} rise with pressure [*Raase*, 1974; *Brown*, 1977; *Holland and Richardson*, 1979; *Spear*, 1980].

[29] The Ca-amphiboles in our samples can be compared with those reported by *Zenk and Schulz* [2004], who provided detailed microstructural, mineral chemical and thermobarometric data on metabasite Ca-amphibole-bearing assemblages from the classical Barrovian metamorphic zones in the Dalradian Group in Scotland. The overall compositional pattern of Ca-amphiboles from Sardinia metabasites are closely similar to those described by *Zenk and Schulz* [2004] for the biotite, or garnet and kyanite zones. As in metabasites in the Dalradian Group, our samples similarly show coexistence of Ca-amphiboles with plagioclase ranging in composition from nearly pure albite to oligoclase (typical of the biotite zone) or, more frequently, with andesine/labradorite (garnet or kyanite zone).

[30] Results of the application of the empirical Ca-amphibole geothermobarometry using the analytical expression given by *Zenk and Schulz* [2004] are listed in Table 2.

[31] The variation ranges of estimated P-T values for E18, E16, MN4b, and A165a are within the absolute error ranges (±0.12 GPa and ±37°C) of the geothermobarometric method.

[32] In samples E6, E10, and E12, there is a wider variability of P-T values which is related to compositional variations of Ca-amphibole grains from different microstructural settings. In sample E6 the highest P and T values (1.02 GPa, 674°C) were obtained using the composition of Fe-pargasite blasts intergrown with plagioclase and ilmenite, whereas the minimum values (0.55 GPa and 565°C) are due to matrix Mg-hornblende far from garnet. In eclogite E10, maximum P and T values (0.80 GPa, 677°C) were similarly given by Fe-pargasite associated with ilmenite or magnetite and plagioclase in coronas around garnet. Minimum values (0.45 GPa, 532°C) were obtained from the late Mg-hornblende crystals which overgrow garnet and the symplectite-rich domains. In retrogressed eclogite E12, maximum P and T values (0.84 GPa, 684°C) were obtained using Fe-pargasite and Fe-hornblende crystals in contact with ilmenite, and minimum P and T (0.28 GPa, 456°C) using the composition of Mg-hornblende blasts far from ilmenite.

6. Magnetic Properties

[33] Fifty to one hundred in situ measurements were recorded for each unweathered outcrop. A bimodal distribution of κ values was detected in P. De Li Tulchi metabasites where highly magnetic eclogites are associated to retrogressed eclogites with low κ values. Among the twelve studied samples the minimum value of apparent magnetic susceptibility is for Erula amphibolites (E18, E19, $\kappa = 0.39 - 0.62 \times 10^{-3}$ SI), while the maximum is for Punta de Li Tulchi eclogite (E10, $\kappa = 11 - 22 \times 10^{-3}$ SI), suggesting the difference in susceptibility to be related to a

Figure 4. Photomicrographs of investigated samples of metabasites from the Medium-Grade Internal Nappe Zone of NE Sardinia. (a) inclusions of rutile (Rt) intergrown with ilmenite (Ilm) within a Ca-amphibole (Cam)-rich matrix (eclogite E16, PPL); (b) ilmenite (Ilm) rimmed by sphene (Ttn) within a Ca-amphibole (Cam)-rich matrix (eclogite E16, BSE); (c) fine-grained aggregate of plagioclase (Pl) and Ca-amphibole (amphibolite E18, PPL); (d) ilmenite (Ilm) associated with Ca-amphibole (Cam) and minor plagioclase (Pl) (amphibolite E18, PPL); (e) anhedral garnet (Grt) porphyroblasts with discontinuous plagioclase (Pl)-rich coronas, set within a nematoblastic matrix of Ca-amphibole and plagioclase (Pl) with scattered ilmenite (Ilm) grains (amphibolite E5, PPL); (f) pyrrhotite (Po) as discrete grains enclosed in garnet (Grt) and in Ca-amphibole (Cam) close to garnet margin (amphibolite E5, BSE); (g) ilmenite (Ilm) intergrown with Ca-amphibole (Cam) and plagioclase (Pl) (amphibolite E6, BSE); (h) ilmenite (Ilm) rimmed by sphene (Ttn) within a plagioclase (Pl)-Ca-amphibole (Cam) matrix (amphibolite E6, PPL).

Table 3. Mineral Magnetic Parameters of Northern Sardinia Metabasites

Sample	Magnetic Susceptibility, 10^{-8} m^3 kg^{-1}	NRM, A m^2 kg^{-1}	ARM, A m^2 kg^{-1}	IRM, A m^2/kg		S Ratio
				900 mT	−300 mT	
E5	67.91	9.51E-05[a]	3.51E-04	3.19E-02	3.30E-02	1.04
E6	97.98	4.24E-05	1.90E-04	2.22E-02	2.21E-02	1.00
E10	1047.7	3.46E-04	3.20E-04	4.34E-02	4.34E-02	1.00
E12	31.16	1.09E-07	1.20E-07	3.86E-06	3.73E-06	0.97
E16	30.82	8.59E-07	1.21E-07	8.35E-06	8.13E-06	0.97
E18	30.03	3.10E-07	5.39E-07	1.83E-05	1.00E-05	0.55
E19	28.71	3.51E-06	1.84E-06	4.08E-05	3.12E-05	0.76
A162a	31.93	2.33E-06	6.49E-07	1.39E-04	1.33E-04	0.96
A165a	12.38	3.48E-06	4.90E-07	1.34E-05	1.27E-05	0.95
MN3b	860.87	6.23E-04	1.50E-04	3.85E-02	3.82E-02	0.99
Mn4b	236.44	2.79E-02	9.38E-04	4.95E-02	4.95E-02	1.00
Mn4e	43.31	1.19E-03	1.85E-05	2.28E-03	2.20E-03	0.96

[a]Read 9.51E-05 as 9.51×10^{-5}.

different metamorphic grade. However, comparing two eclogites, such as the Punta de Li Tulchi one (E10) with the Giuncana one (E16, $\kappa = 0.62-0.85 \times 10^{-3}$ SI), it is evident that is not so straightforward to find an explanation for such a variability (Table 3).

[34] Among measured samples the highest mass specific magnetic susceptibility (χ) value (1047.70×10^{-8} m^3 kg^{-1}) is for E10 (Punta de Li Tulchi eclogite) and the lowest (12.38×10^{-8} m^3 kg^{-1}) is for A165a (Punta Scorno amphibolite) (Table 3). Its variability is not only on a regional scale but also at the outcrop scale as showed by its value at Punta de Li Tulchi: 1047.70×10^{-8} m^3 kg^{-1} for E10, while 31.16×10^{-8} m^3 kg^{-1} for E12 (retrogressed eclogite).

[35] The natural remanent magnetization (NRM) intensity ranges from a minimum of 1.09×10^{-7} A m^2 kg^{-1} for E12 (Punta de Li Tulchi amphibolite) to a maximum of 1.19×10^{-3} A m^2 kg^{-1} for MN4e (Montiggiu Nieddu amphibolite) (Table 3). Intermediate values are in the order of $10^{-6}-10^{-7}$ A m^2 kg^{-1} for Erula (E18, E19) and Punta Scorno (A162a, A165a) amphibolites and for E16 Giuncana eclogite, while of $10^{-4}-10^{-5}$ A m^2 kg^{-1} for Punta Figliacoro (E5, E6) and Montiggiu Nieddu (MN3b) amphibolites and for E10, Punta de Li Tulchi eclogite. It is worth noting that the high NRM intensity value of 1.19×10^{-3} A m^2 kg^{-1} for the Montiggiu Nieddu amphibolite is close to the IRM value for the same sample (see below). This feature, and the site location close to the crest of a topographic high, suggests that this place has been hit by one or more lightning [*Verrier and Rochette*, 2002].

[36] Among selected samples MN4b (Montiggiu Nieddu amphibolite) shows the highest values for artificial magnetizations (IRM $_{900mT} = 4.95 \times 10^{-2}$ A m^2 kg^{-1} and ARM = 9.38×10^{-4} A m^2 kg^{-1}) while E12 (Punta de Li Tulchi retrogressed eclogite) shows the lowest ones (IRM$_{900mT}$ = 3.86×10^{-6} A m^2 kg^{-1} and ARM = 1.20×10^{-7} A m^2 kg^{-1}) (Table 3). The variability in IRM and ARM reflects a different modal content of ferromagnetic minerals: MN4b (together with E10, MN3b, E5, E6, MN4e) contains a higher concentration of ferromagnetic minerals than E12 (together with E16, E19, E18, A165a, A162a), the latter samples being enriched in paramagnetic minerals.

[37] The ratio of IRM-300 mT to IRM 900 mT is defined as S ratio. It can be used to quantify the ratio of hard (magnetized at saturation) to soft (remagnetized in the back field direction) minerals in a sample. A value very close to 1 (>0.95) indicates a high content of low-coercivity ferromagnetic "in a broad sense" minerals instead of high-coercivity ones. Comparing the results for studied samples (Table 3), E18 and E19 (Erula amphibolites) show the lowest values for this parameter demonstrating their highest content in high-coercivity minerals such as hematite. In the other samples S ratio is approximately 1 thus indicating the presence of low-coercivity phases such as magnetite, titanomagnetite, maghemite and pyrrhotite.

[38] All of the investigated samples produce irreversible thermomagnetic curves during cooling (Figures 5 and 6); in some cases, susceptibilities are far higher during cooling compared to the heating curves. This indicates that new magnetic phases were created during heating. For selected samples, temperature dependence of susceptibility was measured in an argon atmosphere in order to minimize mineral reactions with atmospheric oxygen during heating (Figure 5). It is evident for some samples (e.g., E5, E6, E10, A165a) that monoclinic pyrrhotite (Fe_7S_8) is present (T_{Curie} = 320°C) along with minor magnetite. The reducing environment limited magnetite neoformation as a result of iron sulfide oxidation above ~400°C. The presence of pronounced and narrow Hopkinson peaks reflect the presence of pyrrhotite grains with a narrow grain size range [*Dunlop and Özdemir*, 1997]. Samples Mn4b and Mn4e show a similar behavior characterized by a broad peak centered at 260°C and the absence of a peak at 320°C. While the latter indicate the absence of monoclinic pyrrhotite, the broad peak centered at 260°C could indicate the presence of the hexagonal pyrrhotite like Fe_9S_{10} and $Fe_{11}S_{12}$ [*Schwarz and Vaughan*, 1972]. At this stage, we cannot rule out the presence of titanomagnetite that exsolve during heating. A few samples (E12, E16, GA, and A162A) only show a decrease in susceptibility near 580°C, which indicates that magnetite, among the ferromagnetic grains, is the major contributor to magnetic susceptibility (Figure 6). In addition, the very low magnetic susceptibility values associated to its hyperbolic decrease with increasing temperature between ~20°C and 250–350°C is typical for a dominant paramagnetic contribution of mafic silicates. In sample E16 (Giuncana eclogite) we estimated a paramagnetic contribution of 88% ($\kappa_p = 13.89 \times 10^{-6}$ SI) to the total magnetic susceptibility ($\kappa = 15.78 \times 10^{-6}$ SI). These results, as we show in the next paragraph, are confirmed by the analyses

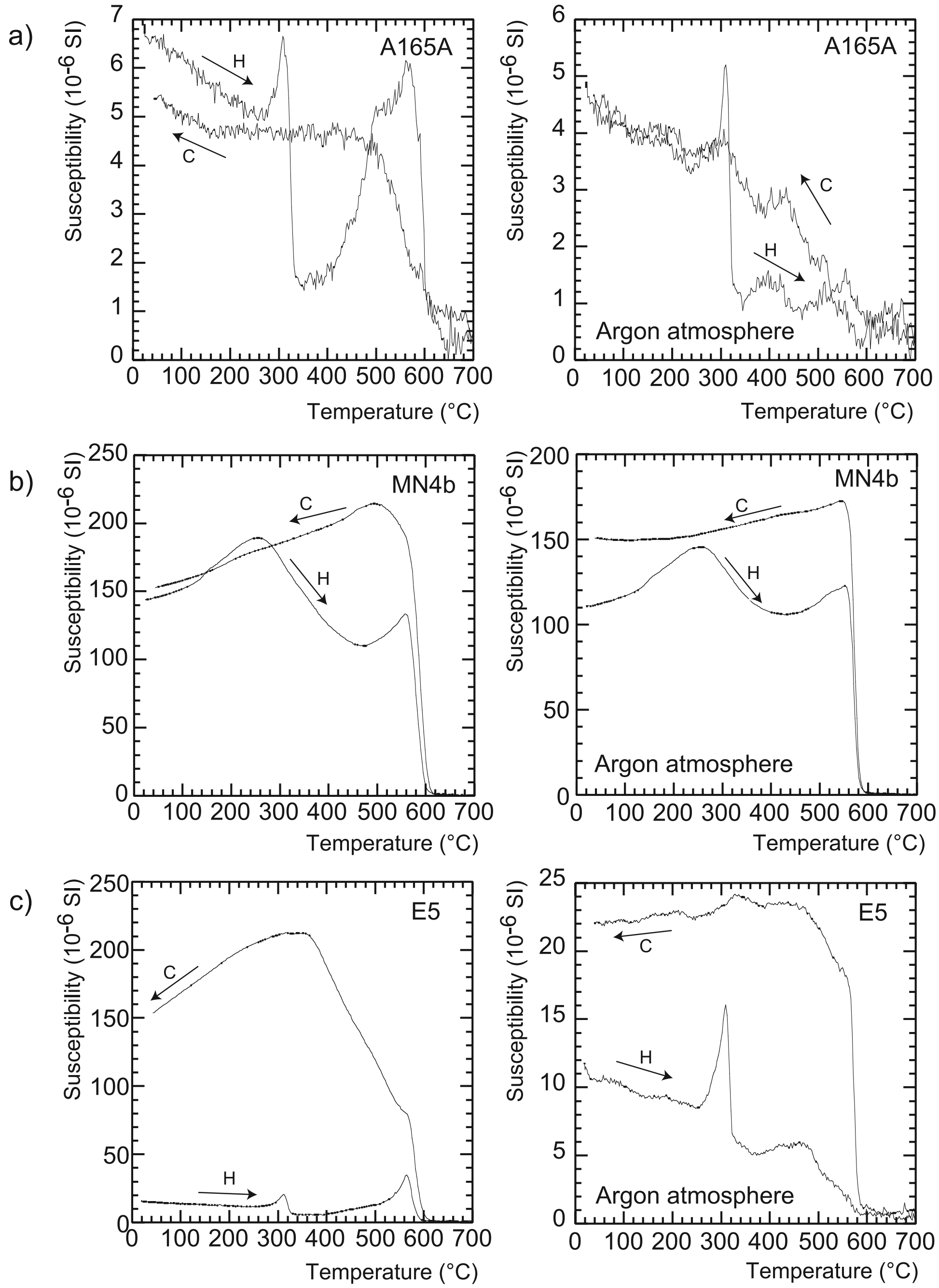

Figure 5. Magnetic susceptibility versus temperature for samples A165a, Mn4b, and E5 in standard conditions and in an argon atmosphere in order to minimize mineral reactions with atmospheric oxygen during heating (see text). The heating and the cooling paths are indicated by H and C, respectively. The data are corrected for the diamagnetism of the furnace.

of high-field magnetization behavior (hysteresis loops) (Figure 7). These four samples show a positive linear relationship between applied field and magnetization typical for paramagnetic behavior.

[39] As mentioned above, samples E16, E12, GA, and A162a have a very high paramagnetic content and this is reflected in the positive linear relationship between applied field and magnetization (Figure 7). Conversely, the remaining studied samples E5, E6, A165a, MN4b, and MN4e are saturated in applied fields of 200–300 mT and show a variety of hysteresis loops shapes, without evidence of "wasp-waisted" characteristics [*Roberts et al.*, 1995]. For each sample with a well-defined loop we determined the saturation magnetization (M_s), saturation remanence (M_{rs}), coercive force (B_c), and coercivity of remanence (B_{cr}). The range of hysteresis ratios found (B_{cr}/B_c versus M_{rs}/M_s) indicate a grain size ranging from single-domain (SD) (ranges from less than $\sim$0.1 μm (cubic magnetite) to $\sim$1 μm (elongate grains)) to pseudosingle-domain (PSD) grains (ranges from less than $\sim$0.1–1 μm (cubic magnetite)

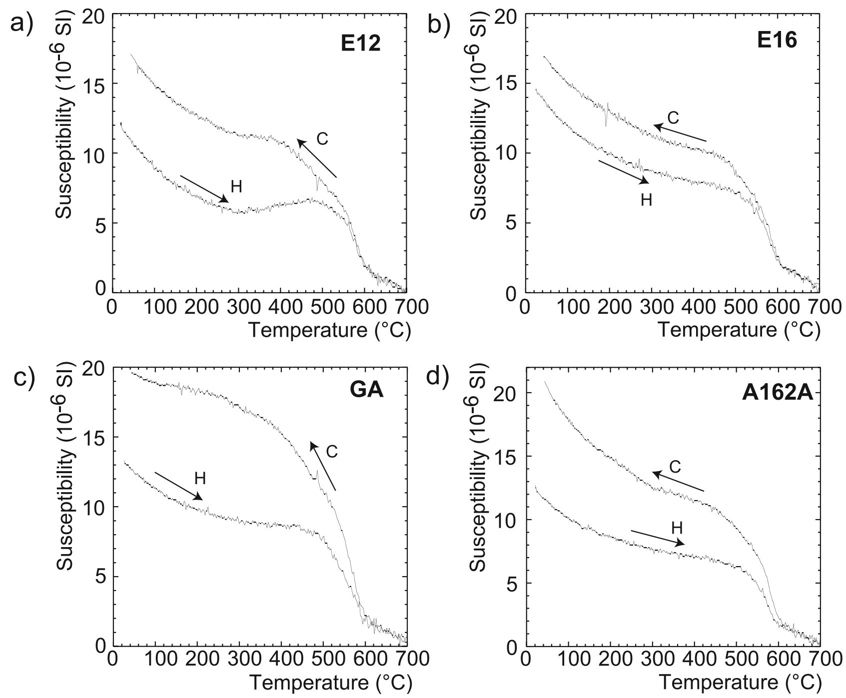

Figure 6. Magnetic susceptibility versus temperature. Samples E12, E16, GA, and A162a only show a decrease in susceptibility near 580°C, which indicates that magnetite, among the ferromagnetic grains, is the major contributor to magnetic susceptibility (see text). The heating and the cooling paths are indicated by H and C, respectively. The data are corrected for the diamagnetism of the furnace.

to about ~15 μm) [*Day et al.*, 1977] (Figure 7). In particular, amphibolites like E5, E6, and A165a contain SD particles, while the remainder eclogite (E10) and amphibolites (MN4b, MN4e) contain PSD particles.

7. Discussion and Conclusions

[40] Magnetic petrology integrates rock magnetism and conventional petrology to characterize the composition, abundance, microstructures and paragenesis of magnetic minerals in order to define the processes that create, alter and destroy magnetic minerals in rocks [*Clark*, 1997; *Dunlop and Özdemir*, 1997; *Frost*, 1991b].

[41] The data collected on the petrographically similar Giuncana eclogites and Punta del Li Tulchi eclogites indicate a significant contrast in magnetic properties which mainly reflect the nonubiquitous occurrence of pyrrhotite, magnetite and/or titanomagnetite in the samples. Moreover, omphacite relics in the high magnetic eclogite from P. de Li Tulchi are characterized by rather high contents of acmite whereas Giuncana omphacites have lower acmite contents. These different omphacite compositions suggest differences in the oxidation ratio of Fe and in the partitioning of Fe^{3+} among silicates and oxides between the two eclogite occurrences during the eclogite facies metamorphism. In both localities the clinopyroxene replacing omphacite is a nearly pure diopside with very low acmite contents. In P. de Li Tulchi eclogites this evidence corroborate the petrographical evidence that Fe^{3+} of omphacite was mainly incorporated in discrete Fe(Ti)-oxides during retrogression, as documented by the abundance of magnetite in these rocks.

[42] Microstructural evidence and compositional data clearly indicate the occurrence of at least three different generations of magnetite in P. De Li Tulchi eclogites: (1) relict titanomagnetite (only as inclusion in garnet cores); (2) fine nearly pure Fe_3O_4 granulations hosted in Ca-amphibole kelyphites or in diopside + albite symplectites (MtI), and (3) a later generation of pure magnetite (MtII) in crystals associated to sphene replacing ilmenite.

[43] The high magnetic Punta de Li Tulchi eclogites show petromagnetic features which are not common in this lithology which, as described by *Clark* [1997], is generally paramagnetic being the stability field of magnetite restricted to P below 1–2 GPa. As stated by *Frost* [1991a] and *Clark* [1997], differences in magnetic properties of meta-igneous rocks can reflect subtle variations in some or all the following factors: the bulk composition and petrogenetic affinities of the magma, the degree of differentiation, conditions of emplacement, degree and type of hydrothermal alteration and conditions of metamorphism (T, P, fugacities of oxygen, water, sulphur, CO_2, etc.). In our samples, since microstructural evidence suggest that the magnetic minerals are either relics of the protolith paragenesis or formed during the posteclogite metamorphic evolution, the different magnetic properties may mainly reflect either the heterogeneous distribution of primary titanomagnetite and pyrrhotite in the protolith, or the variable preservation of these minerals as metastable relics or the formation of neoblastic retrograde magnetite during the subsequent post-peak metamorphic evolution. Titanomagnetite or ilmenite are typical early crystallization products from basaltic/gabbroic rocks [*Frost and Lindsley*, 1991; *Schlinger and*

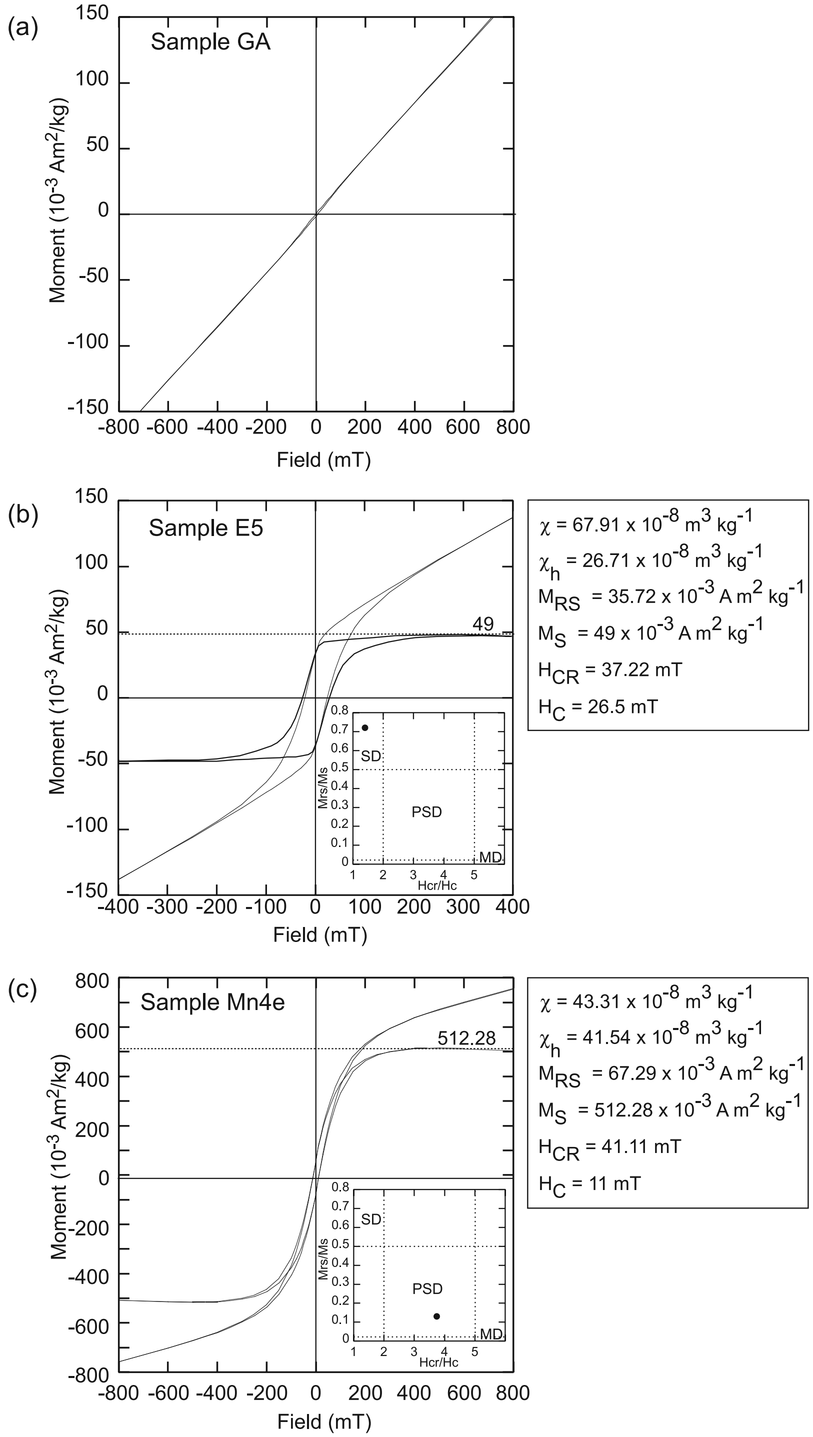

Figure 7. (a) Positive linear relationship between applied field and magnetization for sample GA, which is characterized by a very high paramagnetic content. (b, c) Typical hysteresis loops, magnetic parameters and "Day plots" for two representative samples, before and after correction for the paramagnetic contribution. The range of H_{cr}/H_c versus M_{rs}/M_s ratios indicates a grain size ranging from SD for amphibolite E5 to PSD grains for amphibolite Mn4e.

Veblen, 1989] and titanohematite is also an important mineral for deep crustal magnetization [*McEnroe et al.*, 2001]. For tholeiitic rocks in both oceanic and continental setting iron and titanium-rich variants have been found to show significantly higher susceptibility, reflecting greater modal titanomagnetite, than similar rocks with lower Fe and Ti contents [*Anderson et al.*, 1975; *De Boer and Snider*, 1979]. Bulk rock compositions of Giuncana and Punta de Li Tulchi eclogites [*Cappelli et al.*, 1992] are consistent with this pattern.

[44] In Punta de Li Tulchi (E10) eclogite the study of microstructural relations among opaque minerals and between them and silicatic phases allows a preliminary reconstruction of the sequence of mineralogical transformations involving sulphides and Fe-Ti oxides in these rocks.

[45] In the case of pyrrhotite, as crystals intergrown with rutile and rimmed by ilmenite or magnetite, microstructural relations have been interpreted as the evidence of oxidation and hydratation transformations, according to model reactions like

$$\text{pyrrhotite} + \text{rutile} + O_2 \rightarrow \text{ilmenite} + S_2 \; [\textit{Frost}, 1991\text{b}]$$

$$\text{pyrrhotite} + H_2O \rightarrow \text{magnetite} + H_2S \; [\textit{Frost}, 1991\text{b}]$$

[46] The occurrence of premetamorphic pyrrhotite can be problematic since sulfide minerals are known to equilibrate an order of magnitude faster than silicate minerals [*Barton*, 1970]. However, a study of the prograde and retrograde metamorphism of sulfide minerals in blueschist and eclogite, part of a subduction complex in northern New Caledonia [*Brown et al.*, 2005], indicate that sulfide minerals that became isolated from the matrix as inclusions in prograde porphyroblasts can be effectively armored against external changes in sulfur fugacity and have not been subject to changes induced by retrogression or fluid influx. The presence of pyrrhotite and other sulphides (pyrite, chalcopyrite) is common in granulite facies metabasites from the Ivrea-Verbano Zone [*Wasilewski and Warner*, 1988], and it has been described in very well preserved UHP (>4 GPa) kyanite-bearing eclogites from the Bohemian Massif of the Variscan orogenic belt by *Nakamura et al.* [2004].

[47] Comparison between well-preserved eclogites and retrogressed eclogites at Punta de Li Tulchi indicate a marked variation in magnetic properties over a small area corresponding to a few meters wide outcrop. The marked decrease in magnetic susceptibility from the least to the more retrogressed types indicate that metamorphic reequilibration under high PH_2O amphibolite facies conditions promoted the breakdown of magnetic minerals. This pattern is similar to the one observed by *Skilbrei et al.* [1991] in mafic granulites from central Norway where the reduction of the magnetite content was noted to be due to replacement of magnetite by silicates, mainly hornblende and sphene (also leucoxene) during late retrogression at high PH_2O.

[48] In Punta de Li Tulchi eclogites, in addition to the rare titanomagnetite relics, magnetite is also present in at least two subsequent generations, the first one represented by fine nearly pure Fe_3O_4 granulations hosted in Ca-amphibole kelyphites (MtI), and a later one (MtII) in crystals associated to sphene replacing ilmenite.

[49] When compared to Giuncana eclogites, it is worth to mention that Punta de Li Tulchi eclogites experienced similar peak P-T conditions but partly different postpeak metamorphic trajectory including a granulite facies stage [*Franceschelli et al.*, 1998; *Cortesogno et al.*, 2004]. Additional metamorphic nearly pure magnetite (MtI) could have therefore formed as secondary mineral in the Punta de Li Tulchi eclogite during the postpeak evolution under low PH_2O conditions prior to the amphibolite facies retrogression. The formation of fine-grained magnetite by breakdown of clinopyroxene and garnet during rapid uplift is reported in HP granulites by *Clark* [1997] and by *Skilbrei et al.* [1991], who reported the formation of magnetite during the early retrogression at low PH_2O conditions as result of the breakdown of garnet and clinopyronexes.

[50] In retrogressed eclogites, the presence of abundant ilmenite well dispersed in kelyphites rimming garnet, intergrown with hornblende, often with rutile inclusions, can be interpreted, accordingly with *Franceschelli et al.* [1998], as result of the model reaction:

$$\text{garnet} + \text{clinopyroxene(omphacite)} + \text{rutile} + H_2O \rightarrow \text{hornblende} + \text{plagioclase} + \text{ilmenite}$$

[51] Kelyphitic coronas of plagioclase, amphibole and ilmenite are often observed in several amphibolite samples from Punta Figliacoro outcrops and policrystalline aggregates of these minerals probably represent pseudomorphic products of pristine garnets in Erula metabasites.

[52] As suggested by geothermobarometric estimates, in amphibolite E6 (Punta Figliacoro) and retrogressed eclogite E12 (Punta de Li Tulchi) the crystallization of ilmenite, often associated with Fe-pargasite, occurred under medium-P amphibolite facies conditions (E12, ~0.84 GPa, 684°C; E6, ~1.02 GPa, 674°C).

[53] The latest magnetite generation (MtII) is also documented in Montiggiu Nieddu amphibolites, in which geothermobarometric estimates suggest P-T conditions for hornblende formation of about 0.72 GPa and 611°C. These conditions, consistent with estimates by *Giacomini et al.* [2005] in these rocks, are comparable with the amphibolite facies conditions reported by *Harlov et al.* [2005] for the development, likely along the retrograde path but always at medium grade and high oxygen fugacity conditions, of the reaction:

$$\text{hornblende} + \text{ilmenite} + O_2 \rightarrow \text{sphene} + \text{magnetite} + \text{quartz} + H_2O$$

[54] The results from our combined petrological and petromagnetic study confirm *Carmignani et al.*'s [1994] interpretation that significant volumes of mafic/ultramafic rocks may account for the magnetic anomalies flanking the northeastern part of the Posada-Asinara Line in the Hercynian basement of northern Sardinia [*Cassano et al.*, 1979]. Consistent with the occurrence of dominant low-κ leucogranites in the region [*Gattacceca et al.*, 2004], our results corroborate the hypothesis that highly magnetic metabasites, such as the well-preserved eclogites at Punta di Li Tulchi and M. Nieddu amphibolites, can be expected to be the major sources for these anomalies.

[55] Nevertheless, this study also points out a significant heterogeneity of magnetic properties, even down to the outcrop scale, and therefore simplistic correlations between magnetic properties and lithotype and extrapolations of mapped geology and magnetics of one area to another area, ignoring changes in protolith/metamorphic grade are unreliable. The more refined our understanding and knowledge of the magnetic mineralogy in the various rock units in terms of their specific silicate-oxide petrology, the

more effective and realistic will be the geological interpretation of aeromagnetic anomalies in the region.

[56] **Acknowledgments.** We appreciate the insightful reviews and comments by M. J. Dekkers, M. Jackson, and an anonymous reviewer. We thank Zhu Rixiang for his assistance in measuring thermomagnetic properties in an argon atmosphere at the Institute of Geophysics, Chinese Academy of Sciences, Beijing.

References

Anderson, R. N., D. A. Clargue, K. D. Klitgord, M. Marshall, and R. K. Hishimori (1975), Magnetic and petrologic variations along the Galapagos Spreading Center and their relation to the Galapagos Melting Anomaly, *Geol. Soc. Am. Bull.*, *86*, 683–694.

Arthaud, F., and P. Matte (1977), Détermination de la position initiale de la Corse et de la Sardaigne à la fin de l'orogenesè hercynienne grace aux marqueurs géologiques antémésozoiques, *Bull. Soc. Geol. Fr.*, *19*(4), 833–840.

Barton, P. B. (1970), Sulfide petrology, in *Sulfide Minerals*, *Rev. Mineral.*, vol. 1, edited by P. H. Ribbe, 11 pp. Mineral. Soc. of Am., Washington, D. C.

Brown, E. H. (1977), The crossite content of Ca-amphibole as a guide to pressure of metamorphism, *J. Petrol.*, *18*, 53–72.

Brown, J. L., D. J. Ellis, R. Arculus, and A. Christy (2005), Sulfide metamorphism in blueschist and eclogite, north-eastern New Caledonia, *Eos Trans. AGU*, *86*(52), Fall Meet. Suppl., Abstract V13E-0586.

Buddington, A. W., and D. H. Lindsley (1964), Iron-titanium oxide thermometry oxide minerals and synthetic equivalents, *J. Petrol.*, *5*, 310–357.

Cappelli, B., L. Carmignani, F. Castorina, A. Di Pisa, G. Oggiano, and R. Petrini (1992), A Hercynian suture zone in Sardinia: Geological and geochemical evidence, *Geodin. Acta*, *5*, *1–2*, 101–118.

Carmignani, L., and P. Rossi (1999), Carta geologica e strutturale della Sardegna e della Corsica, scale 1:500,000, Ist. Poligr. e Zecca dello Stato S.p.A., Rome.

Carmignani, L., B. Cappelli, S. Barca, A. Di Pisa, G. Oggiano, and P. C. Pertusati (1992), A tentative geodynamic model of for the Hercynian basement of northern Sardinia, in *Contribution to the Geology of Italy*, *IGCP 276, Newsl. 5*, edited by L. Carmignani and F. P. Sassi, pp. 61–83, Int. Geol. Correl. Programme, Siena, Italy.

Carmignani, L., R. Carosi, A. Di Pisa, M. Gattiglio, G. Musumeci, G. Oggiano, and P. C. Pertusati (1994), The Hercynian chain in Sardinia (Italy), *Geodin. Acta*, *7*, 31–47.

Carosi, R., and R. Palmeri (2002), Orogen-parallel tectonic transport in the Variscan belt of northeastern Sardinia (Italy): Implications for the exhumation of medium-pressure metamorphic rocks, *Geol. Mag.*, *139*(5), 497–511, doi:10.1017/S0016756802006763.

Cassano, E., A. Marcello, R. Nannini, S. Pretti, G. Ranieri, R. Salvadori, and I. Salvadori (1979), Rilievo aeromagnetico della Sardegna e del mare circostante, *Ente Miner. Sardo*, *3–4*, 7–30.

Castorina, F., G. Cesaraccio, A. Di Pisa, and G. Oggiano (1996), The amphibolitic stratified complex of Punta Scorno (Asinara Island, Sardinia, Italy): Petrogenesis and tectonic interpretation, *Plinius*, *16*, 74–76.

Clark, D. A. (1997), Magnetic petrophysics and magnetic petrology: Aids to geological interpretation of magnetic surveys, *J. Aust. Geol. Geophys.*, *17*(2), 83–103.

Cortesogno, L., L. Gaggero, G. Oggiano, and J. L. Paquette (2004), Different tectono-thermal evolutionary paths in eclogitic rocks from the axial zone of the Variscan chain in Sardinia (Italy) compared with the Ligurian Alps, *Ofioliti*, *29*, 125–144.

Cruciani, G., M. Franceschelli, and S. Jungs (2003), Zircon morphology and Pb-Pb dating of amphibolite bearing migmatite from the Variscan chain of NE Sardinia, Italy, paper presented at FIST Geoitalia 2003, Assoc. Ital. di Geol. Appl. e Ambientale, Bellaria, Italy.

Day, R., M. D. Fuller, and V. A. Schmidt (1977), Hysteresis properties of titanomagnetite: Grain size and composition dependence, *Phys. Earth Planet. Inter.*, *13*, 260–267.

De Boer, J., and F. G. Snider (1979), Magnetic and chemical variations of Mesozoic diabase dikes from eastern North America: Evidence for a hotspot in the Carolinas?, *Geol. Soc. Am. Bull.*, *90*, 185–198.

Di Vincenzo, G., F. M. Elter, C. Ghezzo, R. Palmeri, and C. A. Ricci (1994), Petrological evolution of the Palaeozoic basement of Sardinia, in *Petrology, Geology and Ore Deposits of the Palaeozoic Basement of Sardinia*, *Guide-Book to the Field Excursion B3*, edited by L. Carmignani et al., pp. 21–36, Int. Mineral. Assoc., Pisa, Italy.

Dunlop, D. J., and Ö. Özdemir (1997), *Rock Magnetism: Fundamentals and Frontiers*, 573 pp., Cambridge Univ. Press, New York.

Elter, F. M., M. Franceschelli, C. Ghezzo, I. Memmi, and C. A. Ricci (1986), The geology of northern Sardinia, in *Guide Book to the Excursion on the Paleozoic Basement of Sardinia*, *IGCP Project 5 Newsletter*, special issue, edited by L. Carmignani et al., pp. 87–102, casa ed. Pasini, Pisa, Italy.

Ferrara, G., C. A. Ricci, and F. Rita (1978), Isotopic ages and tectonometamorphic history of the metamorphic basement of north-eastern Sardinia, *Contrib. Mineral. Petrol.*, *68*, 1–18.

Franceschelli, M., I. Memmi, and C. A. Ricci (1982), Ca distribution between almandine -rich garnet and plagioclase in pelitic and psammitc schists from the metamorphic basement of north-eastern Sardinia, *Contrib. Mineral. Petrol.*, *80*, 285–295.

Franceschelli, M., I. Turbanti Memmi, A. Eltrudis, R. Palmeri, and G. Carcangiu (1998), Multi-stage metamorphic re-equilibration in eclogitic rocks from the Hercynian basement of NE Sardinia (Italy), *Mineral. Petrol.*, *62*, 3–4.

Franceschelli, M., G. Carcangiu, A. M. Caredda, G. Cruciani, I. Memmi, and M. Zucca (2002), Transformation of cumulate mafic rocks to granulite and re-equilibration in amphibolite and greenschist facies in NE Sardinia, Italy, *Lithos*, *63*, 1–18.

Frost, B. R. (1991a), Magnetic petrology: Factors that control the occurrence of magnetite in crustal rocks, in *Oxide Minerals: Petrologic and Magnetic Significance*, *Rev. Mineral.*, vol. 25, edited by D. H. Lindsley, pp. 489–506, Mineral. Soc. of Am., Washington, D. C.

Frost, B. R. (1991b), Stability of oxide minerals in metamorphic rocks, in *Oxide Minerals: Petrologic and Magnetic Significance*, *Rev. Mineral.*, vol. 25, edited by D. H. Lindsley, pp. 469–488, Mineral. Soc. of Am., Washington, D. C.

Frost, B. R., and D. H. Lindsley (1991), Occurrence of Iron-Titanium oxides in igneous rocks, in *Oxide Minerals: Petrologic and Magnetic Significance*, *Rev. Mineral.*, vol. 25, edited by D. H. Lindsley, pp. 433–468, Mineral. Soc. of Am., Washington, D. C.

Gattacceca, J., J.-B. Orsini, J.-P. Bellot, B. Henry, P. Rochette, P. Rossi, and G. Cherchi (2004), Magnetic fabric of granitoids from southern Corsica and northern Sardinia and implications for Late Hercynian tectonic setting, *J. Geol. Soc. London*, *161*, 277–289.

Ghezzo, C., I. Memmi, and C. A. Ricci (1979), Un evento granulitico nel basamento ercinico della Sardegna nord orientale, *Mem. Soc. Geol. Ital.*, *20*, 23–38.

Giacomini, F., R. M. Bomparola, and C. Ghezzo (2005), Petrology and geochronology of metabsites with eclogite facies relics from NE Sardinia: Constraints for the Paleozoic evolution of southern Europe, *Lithos*, *82*, 221–248.

Harlov, D., P. Tropper, W. Seifert, T. Nijland, and H. J. Forster (2005), The role of fH_2O and fO_2 on the formation of Al-rich Titanite rimes on Ilmenite in amphibolite facies metamorphic rocks: Constraints from equilibria among clinopyroxene-amphibole-magnetite-ilmenite-quartz involving $CaTiSiO_4$ and $CaAlSiO_4OH$, *Geophys. Res. Abstr.*, *7*, 03960.

Helbing, H. (2003), No suture in the Sardinian Variscides: A structural, petrological, and geochronological analysis, Ph.D. thesis, 190 pp., Tübinger Geowiss. Arb., Tübingen, Germany.

Holland, T. J. B., and S. W. Richardson (1979), Amphibole zonation in metabasites as a guide to the evolution of metamorphic conditions, *Contrib. Mineral. Petrol.*, *70*, 143–148.

Kretz, R. (1983), Symbols for rock forming minerals, *Am. Mineral.*, *68*, 277–279.

Leake, B. E., et al. (1997), Nomenclature of amphiboles: Report of the subcommittee on amphiboles of the International Mineralogical Association, commission on new minerals and mineral names, *Can. Mineral.*, *35*, 219–246.

Lecoanet, H., F. Leveque, and S. Segura (1999), Magnetic susceptibility in environmental applications: Comparison of field probes, *Phys. Earth Planet. Inter.*, *115*, 191–204.

McEnroe, S. A., P. Robinson, and P. T. Panish (2001), Aeromagnetic anomalies, magnetic petrology, and rock magnetism of hemo-ilmenite- and magnetite-rich cumulate rocks from the Sokndal Region, South Rogaland, Norway, *Am. Mineral.*, *86*, 1447–1468.

Menot, R. P., and J. B. Orsini (1990), Evolution du socle ante-stephanien de Corse: Evenements magmatiques et metamorphiques, *Schweiz. Mineral. Petrogr. Mitt.*, *70*, 35–53.

Miller, L., F. P. Sassi, and G. Armari (1976), On the occurrence of altered eclogite rocks in north-eastern Sardinia and their implications, *Neues Jahrb. Geol. Paleontol.*, *11*, 683–689.

Nakamura, D., M. Svojtka, K. Naemura, and T. Hirajima (2004), Very high pressure (>4 GPa) eclogite associated with the Moldanubian Zone garnet peridotite (Nové Dvory, Czech Republic), *J. Metamorph. Geol.*, *22*, 593–603.

Papike, J. J., K. C. Cameron, and K. Baldwin (1974), Amphiboles and pyroxenes: Characterisation of other than quadrilateral components and estimation of ferric iron from microprobe data, *Geol. Soc. Am. Abstr. Programs*, *6*, 1053–1054.

Raase, P. (1974), Al and Ti contents in hornblende, indicators of pressure and temperature of regional metamorphism, *Contrib. Mineral. Petrol.*, *45*, 231–236.
Ricci, C. A. (1992), From crustal thickening to exhumation: Petrological, structural and geochronological records in the crystalline basement of northern Sardinia, in *Contribution to the Geology of Italy*, *IGCP 276, Newsl. 5*, edited by L. Carmignani and F. P. Sassi, pp. 187–197, Int. Geol. Correl. Programme, Siena, Italy.
Roberts, A. P., Y. Cui, and K. L. Verosub (1995), Wasp-waisted hysteresis loops: Mineral magnetic characteristics and discrimination of components in mixed magnetic systems, *J. Geophys. Res.*, *100*, 17,909–17,924.
Schlinger, C. M., and D. R. Veblen (1989), Magnetism and transmission electron microscopy of Fe-Ti oxides and pyroxenex in a granulite from Lofoten, Norway, *J. Geophys. Res.*, *94*, 14,009–14,026.
Schwarz, E. J., and D. J. Vaughan (1972), Magnetic phase relations of pyrrhotite, *J. Geomagn. Geoelectr.*, *24*, 441–458.
Skilbrei, J. R., T. Skyseth, and O. Olesen (1991), Petrophysical data and opaque mineralogy of high-grade and retrogressed lithologies: Implications for the interpretation of aeromagnetic anomalies in northern Vestranden, central Norway, *Tectonophysics*, *192*, 21–31.
Spear, F. S. (1980), NaSi-CaAl exchange equilibrium between plagioclase and amphibole: An empirical model, *Contrib. Mineral. Petrol.*, *80*, 140–146.
Speranza, F., I. M. Villa, L. Sagnotti, F. Florindo, D. Cosentino, P. Cipollari, and M. Mattei (2002), Age of the Corsica-Sardinia rotation and Liguro-Provençal Basin spreading: New palaeomagnetic and Ar/Ar evidence, *Tectonophysics*, *347*, 231–251.
Stampfli, G. M., J. von Raumer, and G. D. Borel (2002), Palaeozoic evolution of pre-Variscan terranes: From Gondwana to the Variscan collision, *Spec. Pap. Geol. Soc. Am.*, *364*, 263–280.
Triboulet, C. (1992), The (Na-Ca) amphibole-albite-chlorite-epidote-quartz geothermobarometer in the system S-A-F-M-C-N-H2O. 1. An empirical calibration, *J. Metamorph. Geol.*, *10*, 545–556.
Verrier, V., and P. Rochette (2002), Estimating peak currents at ground lightning impacts using remanent magnetization, *Geophys. Res. Lett.*, *29*(18), 1867, doi:10.1029/2002GL015207.
Wasilewski, P., and R. D. Warner (1988), Magnetic petrology of deep crustal rocks- Ivrea zone, Italy, *Earth Planet. Sci. Lett.*, *87*, 347–361.
Zenk, M., and B. Schulz (2004), Zoned Ca-amphiboles and related P-T evolution in metabasites from the classical Barrovian metamorphic zones in Scotland, *Mineral. Mag.*, *68*(5), 769–786.

F. Florindo, Istituto Nazionale di Geofisica e Vulcanologia, Via di Vigna Murata 605, I-00143 Rome, Italy. (florindo@ingv.it)

E. Strada and F. M. Talarico, Dipartimento di Scienze della Terra, Università di Siena, Via Laterina 8, I-53100 Siena, Italy.